NRC Research Press

ARTICLE

Handling techniques for channel spectra in synchrotron-based Fourier transform spectra[1]

Amr Ibrahim, Adriana Predoi-Cross, and Chad Povey

Abstract: Recently, the high radiance of synchrotron sources has been used to enhance FTIR spectrometer performance. However, excessive channel spectra when synchrotron sources are used degrade the quality of retrieved spectral parameters. We have investigated seven different techniques for handling channel spectra. These techniques were used to reduce channel spectra for a test group of seven samples of CO_2 mixed with air recorded using the synchrotron source at the Canadian Light Source. The increases in signal to noise ratio (SNR) of spectra handled with each technique were calculated. SNR results showed that transmission spectra, produced using synthetic background spectra with simulated channel spectra, achieved the highest SNR improvement. However, when the spectra groups were fitted using a nonlinear least square fit algorithm, the technique using channel spectra fitting produced the smallest fitting residual. Moreover, the retrieved intensities and air broadening coefficients of 21 spectral lines showed that the spectral fitting technique produced the most accurate values as compared to the HITRAN 2008 database (Rothman et al. *J. Quant. Spectrosc. Radiat. Transfer*, **110**, 533 (2009)). Although the spectral fitting technique was accurate in retrieving spectral line parameters, applying the technique at wider spectral ranges reduced this accuracy.

PACS Nos.: 33.20.–t, 33.20.Ea, 33.70.Jg, 32.70.Jz.

Résumé : Récemment, la haute luminance des sources synchrotron a été utilisée pour augmenter la performance des spectromètres FTIR. Cependant, l'excès de spectres cannelés, lorsque des sources synchrotron sont utilisées, dégrade la qualité des paramètres spectraux récupérés. Nous avons étudié sept techniques différentes pour gérer les spectres cannelés. Ces techniques ont été utilisées pour réduire les spectres cannelés dans une série de tests impliquant sept échantillons de CO_2 mélangé à de l'air, enregistrés au Centre Canadien de Radiation Synchrotron. Nous avons calculé l'amélioration du rapport signal sur bruit (SNR) pour chaque technique. Les résultats SNR montrent que les spectres de transmission, produits en utilisant des spectres de fond (background) avec des spectres cannelés simulés, montrent la meilleure amélioration SNR. Cependant, lorsque nous faisons un lissage des groupes de spectres en utilisant un algorithme non linéaire de moindres carrés, la technique qui utilise le lissage des spectres cannelés a produit le plus petit résidu de lissage. De plus, les intensités mesurées et les élargissements de raie dues à l'air de 21 raies spectrales montrent que la technique de lissage des spectres cannelés produit les valeurs les plus précises lorsque comparées à la base de données HITRAN 2008 (Rothman et al. *J. Quant. Spectrosc. Radiat. Transfer*, **110**, 533 (2009)). Même si le lissage des spectres cannelés est précis dans la récupération des paramètres des raies spectrales, son application à des domaines spectraux plus larges réduit cette precision. [Traduit par la Rédaction]

1. Introduction

In spite of all its advantages, there is one major drawback that can make the signal to noise ratio (SNR) of recorded Fourier transform spectra decline, namely the phenomenon of channel spectra, sometimes called "fringing". Channel spectra are the result of extra interferences between light beams inside the FTIR spectrometer in addition to the main interference that occurs at the zero path difference (ZPD) position. These additional interferences create extra interference patterns called "spikes" or "signatures". These problem spikes are generally located near the central interference pattern that occurs when the FTIR spectrometer mirror is at the ZPD position. As any localized feature in the interferogram space will result in sinusoidal waves in the spectrum space upon Fourier transformation, these spikes transform into periodic intensity changes in the baseline of the generated spectrum. The presence of channel spectra in our spectrum creates difficulties in analysing and modeling the recorded spectra to extract the required spectral parameters accurately. These spikes in the interferograms producing channel spectra can be attributed to two possible sources.

The first source for channel spectra, which is unique to FTIR spectrometers using synchrotron sources, arises from the need to inject electron current into these sources on a regular basis to balance the energy dissipated by the synchrotron radiation. During these current injections, the orbit of the electron beam moves considerably, changing the synchrotron radiation direction. This movement changes the radiation path length and direction in the spectrometer, causing a transient spike in the detector response that is recorded in the interferogram data [1]. The second source can be traced back to extra interferences between beams reflected by any of the spectrometer optical components (windows, beam splitters, etc.) or the optical components of the transfer optics when using external sources (as in the case of synchrotron sources). These extra interferences produce additional interference patterns that have a different ZPD than the spectrometer ZPD; therefore these extra interference patterns (spikes) are

Received 31 January 2013. Accepted 21 June 2013.

A. Ibrahim. Alberta Terrestrial Imaging Centre, Department of Physics and Astronomy, University of Lethbridge, 4401 University Drive, Lethbridge, AB T1K 3M4, Canada; Physics Department, University of Alberta, Edmonton, Canada.
A. Predoi-Cross and C. Povey. Alberta Terrestrial Imaging Centre, Department of Physics and Astronomy, University of Lethbridge, 4401 University Drive, Lethbridge, AB T1K 3M4, Canada.
Corresponding author: A. Predoi-Cross (e-mail: Adriana.predoicross@uleth.ca).

[1]This manuscript is part of the special issue Mid- and Far-Infrared Spectroscopy: Techniques and Applications published in memoriam of our colleague Arvid Schultz.

located in the vicinity of the main ZPD interference pattern of the spectrometer.

Despite difficulties in the use of synchrotron radiation in the far-infrared, further improvements of the SNR for synchrotron sources are explored through different techniques. Examples of these techniques include using edge radiation to extract the radiation from the extremities of the bending magnets. Edge radiation produces a beam with similar intensity to the bending magnet radiation but with a smaller angular size than the natural opening angle, therefore increasing the beam's brightness [2]. Another technique to increase the SNR is the use of the coherent summation of synchrotron radiation (CSR) operation mode [3]. In the CSR operation mode, the length of synchrotron electron bunches is reduced by varying the parameters of the accelerator so that the bunch length is of the same order as the far-infrared wavelength range leading to the coherent addition of photon bunches. Recent results showed that the CSR mode can increase the beam intensity by four orders of magnitude at the CLS far-infrared beam line [3]. However the effect of increased coherency on increasing the channel spectra has not been studied.

Another approach to enhance synchrotron performance is the use of the top-off operation mode. This mode of operation attempts to compensate the reduction of synchrotron radiation with time due to the decay of the storage ring current. Usually, synchrotron facilities operate in decay mode in which the initial storage ring current decays to near half of its original value before a new current injection is made [1]. This usually requires current injection two or three times a day. During this long period between injections (8 or 12 h), the decaying current and radiation intensity can produce thermal instabilities in the beamline optics. Therefore, top-off mode, in which the electron beam is quasi-continuously injected into the storage ring to conserve the ring current value, can reduce these instabilities. However, this mode of operation could give rise to spikes in the interferogram. Recently, Vernoud et al. [1] proposed using either a feedback mirror to lock the infrared beam into the sample at slow injection rates or a gating system at high injection rates to interrupt interferogram collection during injections. The gating method cannot work effectively at high spectral resolution because the prolonged time required to record the scans is longer than the time interval between current injections.

The only option left after exhausting all the possible techniques for preventing channel spectra is to try removing them from the recorded spectrum. The term "correcting" would imply that we can remove the channel spectra completely. However, because we are trying to minimize its impact on the quality of spectra, the term handling will be used herein instead. The ultimate goal of any handling technique is to minimize these periodic variations in the baseline of the spectra without distortion of the spectral line parameters, such as line shapes, positions, and intensities.

In this study, we explored two categories of these handling techniques. The first one attempts to remove the channel spectra by modifying the interferogram to remove the spikes causing channel spectra with the least possible impact on the final spectrum. In the second category, signal processing techniques, such as filtering, convolution, and fitting, are used separately or in combination to separate the contribution to the recorded interferogram or spectrum from the instruments' internal reflections and interferences.

2. Channel handling techniques

2.1. Interferogram editing techniques

These handling techniques utilize the fact that the channel spectra result from localized spikes (sometimes called side bursts) in the recorded interferograms. Removing these features from the interferogram will produce a spectrum free of channel spectra upon Fourier transformation. The removal of problem spikes can be achieved by replacing the interferogram segments containing them with zeros or straight line interpolations [4, 5]. However, this approach has the disadvantage of producing sharp discontinuities in the interferogram, which lead to phase errors [4]. It also causes a loss of spectral information in the severed segment. Another approach for removing these spikes is based on the relationship between peak positions of the channel spectra $\tilde{\nu}_m$ and the refractive index of the optical component producing them [4]

$$\tilde{\nu}_m = \frac{m}{2nd} \tag{1}$$

where m = 0, 1, 2, …, and n is the refractive index of the optical component that produces the channel spectra. Equation (1) shows that a small change in the sample thickness, d, will cause a change in the channel spectra peak position, which results from a shift in the spike's position in the interferogram. In cases where the source of the channel spectra can be traced back to the sample (such as, for a thin film sample), slight changes to the sample thickness achieved by titling the sample will make these spikes in the interferogram shift. Replacing the spikes with the corresponding segments from a shifted interferogram will account for the missed information in the spike segments. However, this technique cannot be used in gas spectroscopy because sources of channel spectra cannot be rotated. In addition, when the source of these channel spectra is not the sample itself, this technique cannot be used. Nevertheless, the simple method of replacing the spikes by zeros or straight lines remains a common practice because the removed segment points usually represent a very small percentage of the interferogram points, especially in high-resolution spectroscopy.

On the other hand, many other techniques attempt to avoid the sharp discontinuities resulting from spike removal. For example, a Gauss reduction function could be used to reduce the amplitude of the spikes while reducing the sharp discontinuities at the edges. Following the same principle, we replaced the spikes by polynomial fits of the spikes. The polynomial fit of the spikes produces a very low-resolution image of the spike with much lower amplitude. This curved polynomial line can smooth the sharp transition at the spike boundaries.

We also used the technique introduced by Mellau and Winnewisser [6] to remove channel spectra by producing a synthetic background that contains the same channel spectra as the recorded sample spectrum. This was achieved by editing the sample interferogram replacing all of it with zeros except at the central burst and the spikes. This modified interferogram undergoes a fast Fourier transform (FFT) to produce a background spectrum that has similar channel spectra to the sample spectrum. Then, the channel spectra should cancel out when we use this background to create the transmission spectrum.

2.2. Signal processing techniques

The literature includes many other techniques for handling channel spectra, such as frequency filtering [7, 8], and the utilization of convolution methods to remove them [9, 10]. In this work, we utilized a multispectrum fitting technique that allows the user to analyse several spectra simultaneously over a relatively narrow wavelength interval.

Narrow wavelength intervals are used to avoid any significant refractive index changes within the wavelength range, as these changes will cause changes in the peak position and spacings of channel spectra. Also, the amplitudes of channel spectra show considerable change with wavelength, as a direct result of the wavelength dependence of beam splitter reflectance and transmittance. For example, beam splitters that are free-standing, non-absorbing, parallel-sided, and made of thin dielectric materials have a reflectance R_o and transmittance T_o given by [11]

Fig. 1. Graphical interface of the LabVIEW program used in reading the data file from OPUS and estimating the spike locations manually.

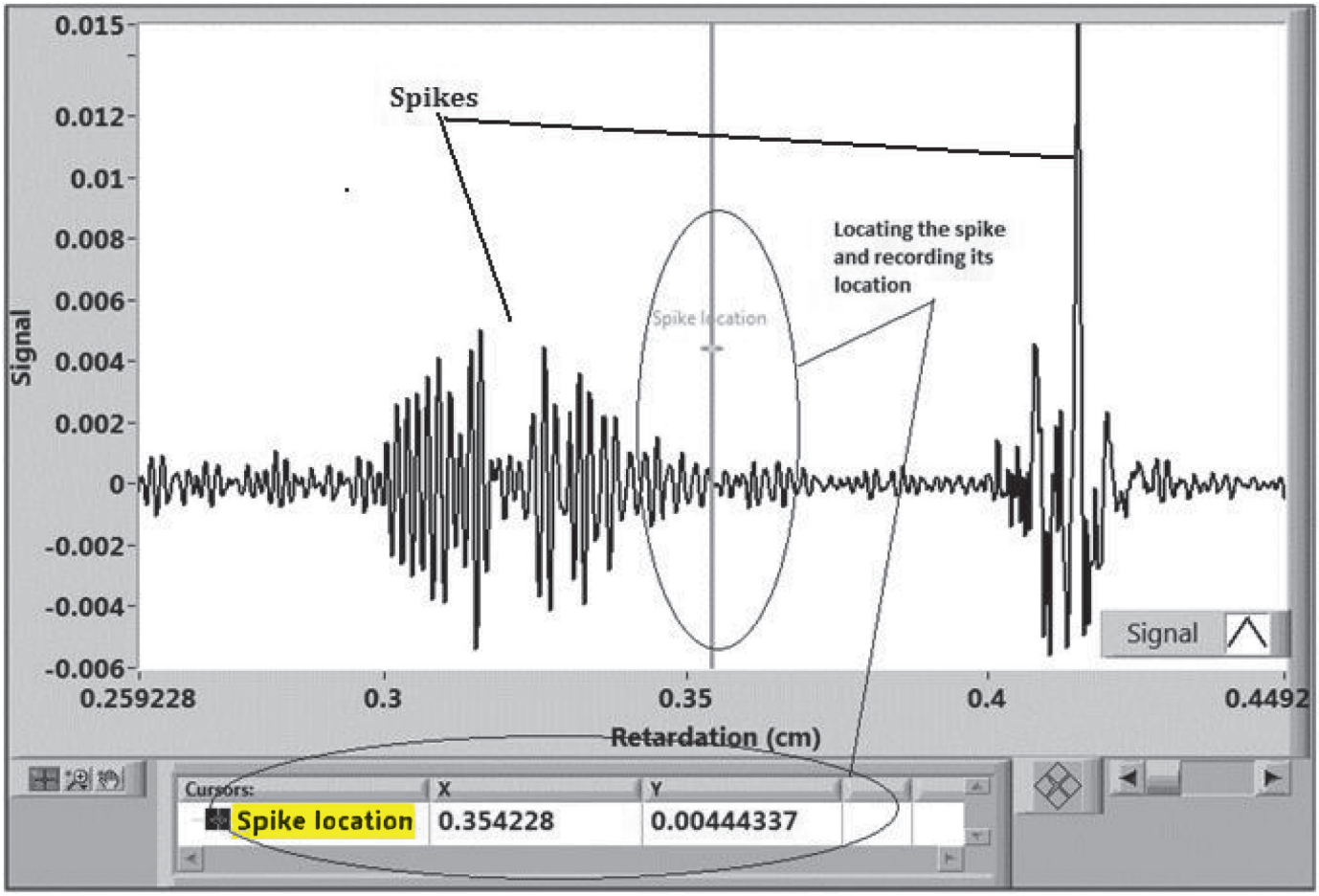

$$R_o = \frac{2R^2(1 - \cos\delta)}{1 + R^2 - 2R\cos\delta} \tag{2}$$

$$T_o = \frac{(1 - R)^2}{1 + R^2 - 2R\cos\delta} \tag{3}$$

where $\delta = 4\pi\tilde{\nu}nd(\cos\theta_t)$ is the relative phase shift (in radians) between two adjacent emerging rays, $\tilde{\nu}$ is the wavenumber, n is the refractive index, d is the thickness of the film, θ_t is the angle between the beam inside the film to the surface normal, and R is the single-bounce reflectance of the material. This wavelength dependence of the channel spectra peak positions, spacings, and intensities complicates the modeling of channel spectra over the complete wavelength range of the recorded spectra. Therefore, within narrow wavelength intervals, we can assume that all optical components have relatively constant refractive indices.

A multispectrum nonlinear least square fitting program is used to fit these segments with initial estimates for the spectral line parameters from the HITRAN database. The complete details of this program can be found elsewhere [12, 13]. In this multispectrum program [12], to calculate the fitted spectrum S as a function of wavenumber $\tilde{\nu}$, the fitted spectrum is calculated from the continuum [100% transmittance level] $B(\tilde{\nu})$, channel spectra $C(\tilde{\nu})$, gas spectrum convoluted with the instrumental line shape $b(\tilde{\nu})$, and zero level offset z as [12]

$$S(\tilde{\nu}) = B(\tilde{\nu})C(\tilde{\nu})b(\tilde{\nu}) + z \tag{4}$$

The change of the fitted spectrum because of the existence of channel spectra is expressed by the derivative of (4) using finite differences [12]

$$\frac{\partial S(\tilde{\nu}, q)}{\partial q} \cong \frac{S(\tilde{\nu}, q + \varepsilon) - S(\tilde{\nu}, q)}{\varepsilon} \tag{5}$$

where q is the parameter with respect to which the derivative is to be taken and ε the change in the quantity q, which is small enough that the derivative of S with respect to q is not significantly different at q, and $q + \varepsilon$, but large enough to avoid precision errors during mathematical operations. When fitting the channel spectra parameters, the derivative of the spectrum with respect to the channel spectra parameters is expressed as

$$\frac{\partial S(\tilde{\nu})}{\partial q} = B(\tilde{\nu})b(\tilde{\nu})\frac{\partial C(\tilde{\nu})}{\partial q} \tag{6}$$

Both $B(\tilde{\nu})$ and $b(\tilde{\nu})$ are calculated for the nominal case. The derivatives of the channel spectrum $C(\tilde{\nu})$ can be determined and used in the fitting process as shown by Benner [12].

3. Implementing channel spectra handling techniques

As mentioned earlier, we divided common channel spectra handling techniques into two groups: (*i*) interferogram editing and

Fig. 2. (A) Original problem spike, (B) replaced by zeros (technique 1), (C) replaced by a straight line (technique 2), (D) replaced by a polynomial curve fit (technique 3), (E) reduced in amplitude (technique 4), and (F) reduced by a Gauss function (technique 5).

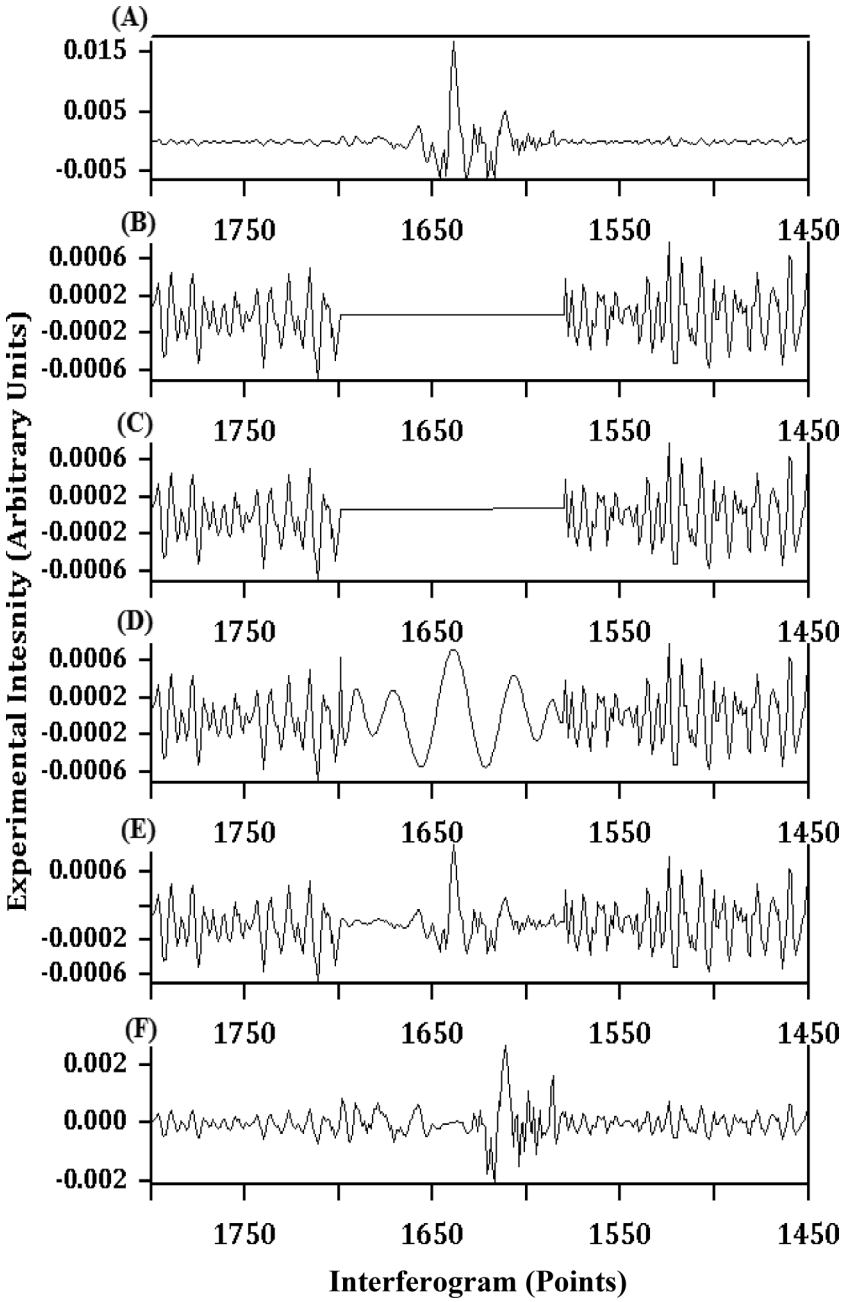

(*ii*) signal processing techniques. LabVIEW software was used to unify the data handling procedures for the different approaches. Although LabVIEW is historically known to be used in instrumentation applications, its graphical programming environment and library of signal processing tools are making it increasingly popular in signal processing applications. The data were recorded by a Bruker FTS125HR spectrometer and were stored in the OPUS file format. The OPUS software was used to average the recorded scans and to remove the displaced interferograms, which can cause spurious channel spectra [14]. Next, we used the OPUS software to produce single-side interferograms and save them in the standard data point table (dpt) file format, then used LabVIEW code to read it as a number array for processing.

In the interferogram editing approach, single-sided interferogram data were used as input for the LabVIEW program to find the locations of problem spikes manually, as shown in Fig. 1. The manual determination of these locations was chosen to avoid with confidence any problems with identifying the spikes responsible for the channel spectra and to ensure that the same spike locations are used for every technique. The spike positions were used as input to another LabVIEW channel handling program. This program contains six subprograms each of which processes the data with a different technique. The six interferogram editing techniques used are:

1. replacing the spikes with zeros,
2. replacing the spikes with a straight line interpolation,

Fig. 3. Synthetic background produced from the sample interferogram.

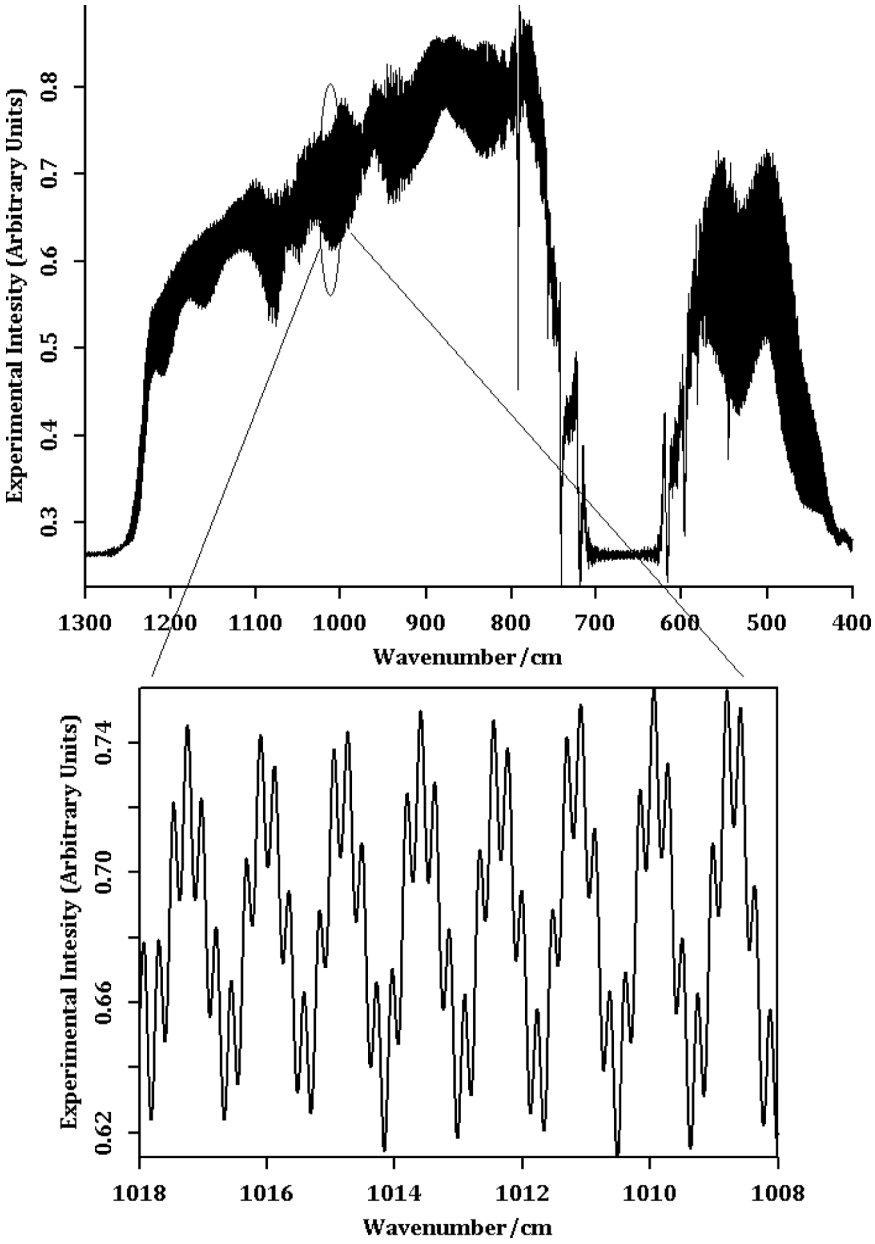

Table 1. Brief description of tested channel handling techniques.

Tech. no.	Method description
0	No channel handling technique is applied
1	Replacing the spikes with zeros
2	Replacing the spikes with a straight-line interpolation
3	Replacing them with a polynomial fit for the spikes
4	Rescaling spikes
5	Reducing spikes by a Gauss function
6	Using synthetic background
7	Fitting channel spectra

Table 2. Description of spectra used in handling technique comparison.

No.	Pressure (Torr)	Temp. (°C)	Resolution (cm^{-1})	Aperture (mm)	No. of scans averaged
1	60.004	23.4	0.003	1.5	289
2	90.010	23.33	0.003	1.5	304
3	201.09	23.31	0.004	1.7	347
4	300.12	23.21	0.004	1.7	423
5	450.42	23.55	0.004	1.7	461
6	525.00	23.82	0.004	1.7	558
7	825.01	23.88	0.004	1.7	472

Note: All samples were CO_2+air.

3. replacing the spikes with polynomial fit for the spikes,
4. reducing the spike amplitude,
5. reducing the spike's amplitude by a Gauss reduction function, and
6. replacing the interferogram points with zeros except for the ZPD and spikes.

In the replacing by zeros subprogram, the spike data point segments were separated using the subarray routine in LabVIEW.

Table 3. Experimental settings used in recoding the CLS spectra.

Cell base length	2 m	Detector	Ge:Cu (300–1850 cm^{-1})
Optical path length	72.15 m	Detector filter	490–1190 cm^{-1}
Windows (range)	KBr (400–5000 cm^{-1})	Beam splitter	Ge/KBr (400–4800 cm^{-1})
Spectral range	450–1200 cm^{-1}	Scan velocity	40 KHz

Fig. 4. Section of the original and handled spectrum using interferogram editing techniques 1–6.

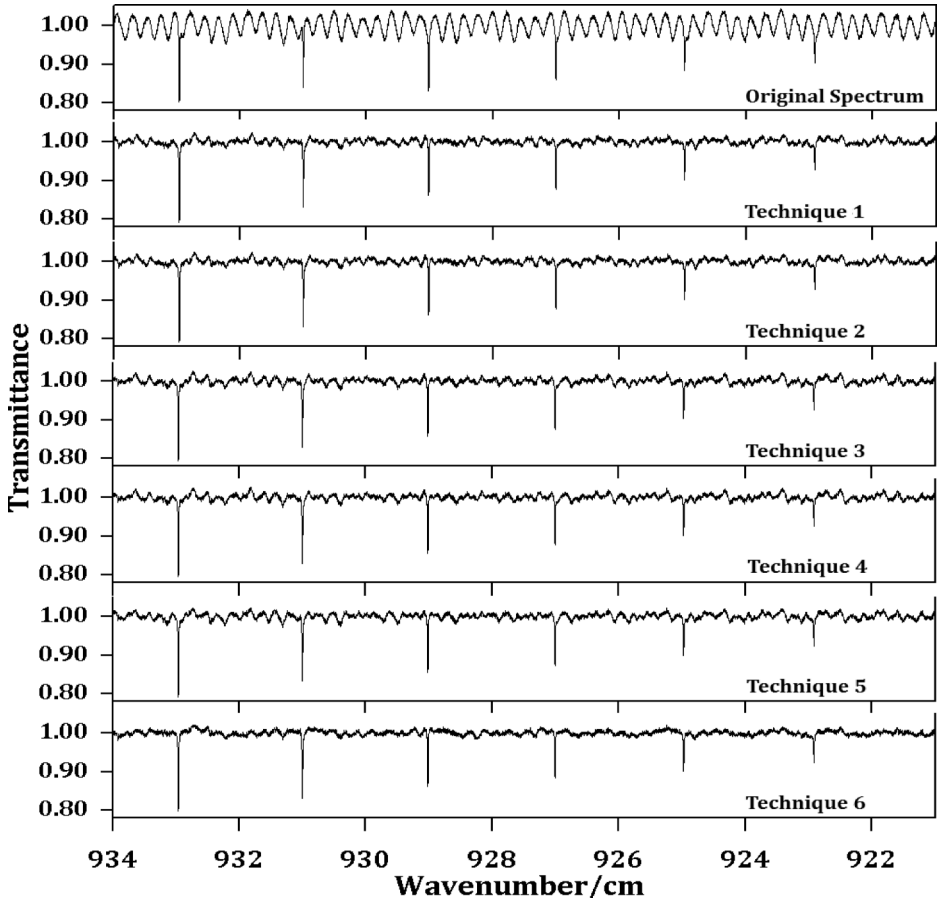

These subarray routines in LabVIEW replace the segments of the interferogram defined by the spike limits with zeros. In the replacement by straight line subprogram, a procedure similar to the one used in the previous subprogram was used. The spike segments were replaced by straight lines interpolated between their limits employing the curve fitting procedure in LabVIEW.

In the polynomial fit subprogram, each problem spike segment was fitted using a fifth degree polynomial function. Also, the peak-to-peak amplitude of the region around the spike was calculated and averaged and then used to rescale the fitted polynomial curve so that it matched the surrounding interferogram segment. The resulting polynomial fitted curve was used to replace the problem spikes. A similar program to the previous one was used to rescale the spike amplitude and reduce it to the levels of the neighbouring interferogram segment. This rescaled spike replaced the original spike in the interferogram. In the Gauss reduction subprogram, the spike segments were extracted from the interferogram and, using an asymmetrical Gaussian window routine in LabVIEW with the spike segment points X as input, we produced modified segments Y fitted to Gaussian curves using

$$Y_i = X_i \exp\left[-\frac{(i-m)^2}{2(\sigma n)^2}\right] \quad \text{for} \quad i = 0, 1, \ldots, n-1 \tag{7}$$

where n is the number of elements in X, $m = (n-1)/2$, and σ is the standard deviation of the Gaussian window. The new segment was subtracted from the spike to produce a Gauss reduced spike that replaced the original one. The same steps were applied to all of the problem spikes. An example of a problem spike that was handled by each of the previous techniques is shown in Fig. 2. Finally, the synthetic background subprogram produced a background spectrum with identical spikes by replacing the interferogram points, except the ZPD and problem spikes, with zeros. The resulting background spectrum, as shown in Fig. 3, was used to create a transmission spectrum with reduced channel spectra.

In the signal processing technique, the data were initially fitted using data from the HITRAN database [15] using the nonlinear least square algorithm described earlier. The resulting fitting residuals have the channel spectra structure. These residual files were analysed using a LabVIEW program that was developed. The program employs a FFT to transform these residuals from the

Fig. 5. Change in the SNR of the spectra of sample 1 handled for channel spectra using interferogram editing techniques.

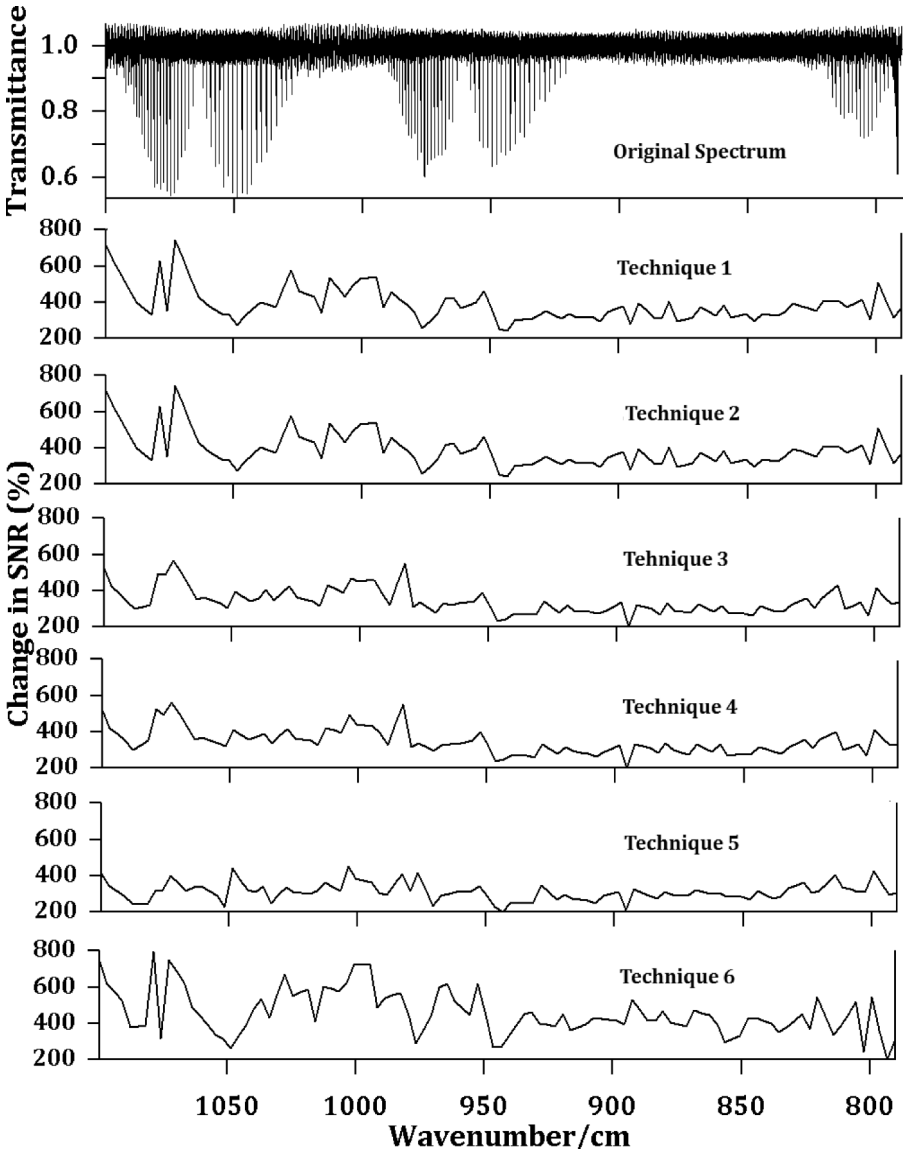

time domain to the frequency domain. Next, the program isolates frequency components with amplitude higher than a user-specified threshold. These threshold limits are used to avoid measuring the noise components, and to limit measurements to channel spectra only. After isolating the targeted frequency components, the program then estimates the individual amplitude, frequency, and phase for each channel separately. These estimated parameters were implemented in the fitting program to model the channels and refit the spectrum intervals again, using the corresponding channel parameters for each interval.

4. Testing and comparing handling techniques

The six different interferogram editing techniques plus the spectral fitting technique discussed in the previous section are listed with brief descriptions in Table 1. For simplicity each technique is labeled in the graphs and results with its corresponding technique number.

As mentioned earlier, the SNR is considered to be an indicator of the quality of the measured spectra and is related to channel spectra. The highest achievable SNR in a spectrum is limited by the original noise in the interferogram. To test the channel handling techniques, we developed a LabVIEW program to calculate the SNR of the spectra handled for channel spectra. To calculate SNR, the program reads the transmission spectra and calculates SNR as the average of these data within prespecified intervals divided by the standard deviation of the data at base line points. The program calculates the SNR at prespecified intervals between spectral lines to avoid calculation errors when lines broadened at high pressure are included in the SNR interval. Our calculation used the baseline of the transmission as the signal (ideally equal to 1) to study the change of SNR with wavelength.

To study the effect of handling techniques on spectra with different line parameters, seven synchrotron source spectra were chosen for comparisons. A detailed description of these sample spectra is listed in Table 2 and the experimental settings of the measurements are shown in Table 3. All channel handling techniques (except method 7) were applied to every spectrum and the SNR before and after channel handling was calculated. Method 7 was not included in the SNR analysis because it did not

Fig. 6. Change in SNR with interferogram editing techniques for samples 2 and 3.

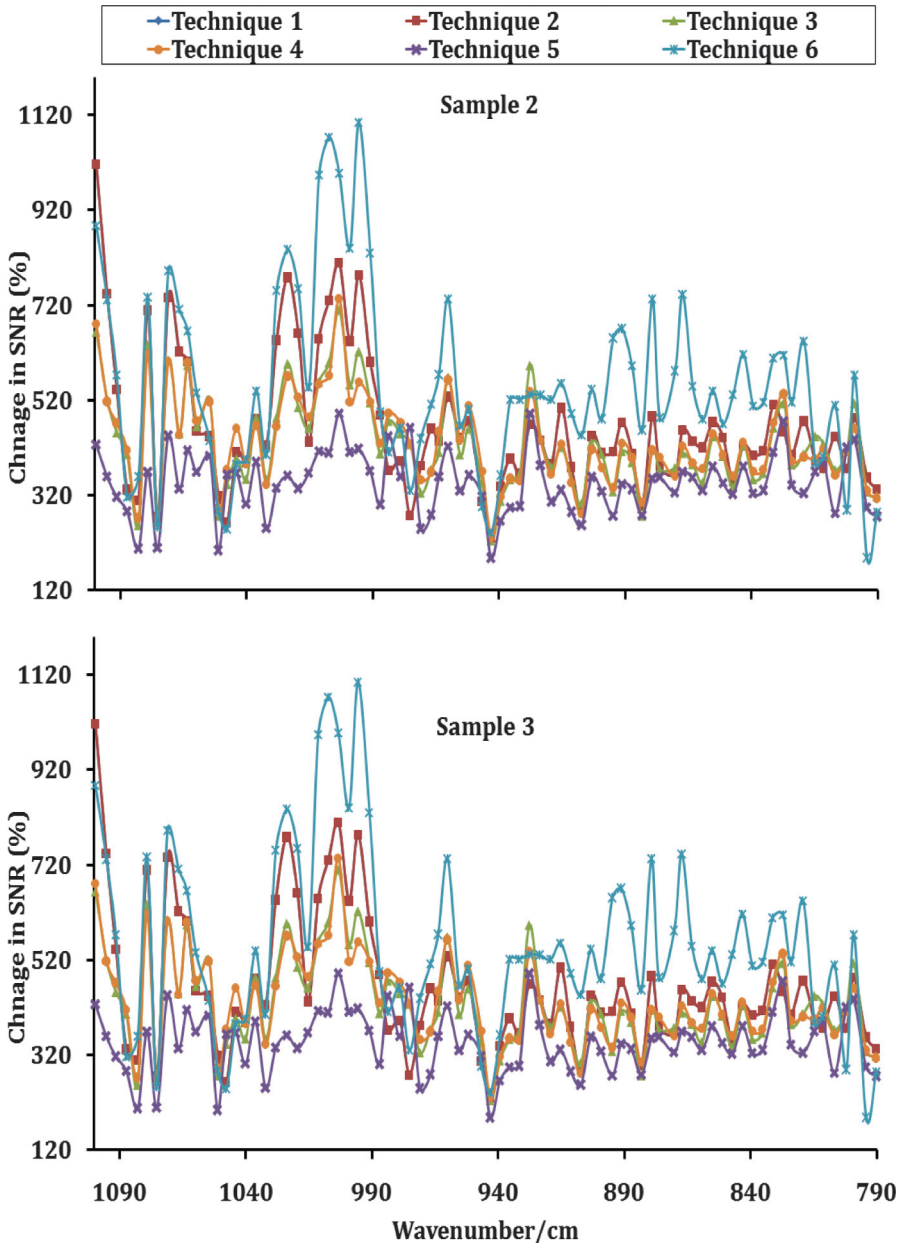

modify or change the original spectrum but helped to better model it. A section of sample 1 handled spectra is shown in Fig. 4.

It is difficult to show the difference between results from the different handling techniques by examining the stacked spectra of sample 1 shown in Fig. 4. However, the percentage SNR change [(SNR after handling/SNR before handling)*100] shown in Fig. 5 can provide us with some useful observations. All spectra SNR seem to be dependent on the wavelength, which can be attributed to the channel spectra amplitude dependence on wavelength (see (1), (2), and (3)). Also, Fig. 5 shows that technique 6 (synthetic background) achieves better improvements than the other techniques. For example, the increasing in SNR of example 1 spectrum handled by technique 6 was 18%[2], 18%, 34%, 33%, and 47% higher than techniques 1–5, respectively. We can also notice that techniques 1 and 2 produce almost the same results, as expected because they are quite similar techniques. Examining sample 2–7 spectra in Figs. 6–8, we see that technique 6 has better SNR improvement in all samples except sample 7. This difference of sample 7 can be attributed to imprecision in the spike locations, which results in a synthetic background with different channels of the sample spectrum. Improvements in technique 6 could be achieved by iteration of changing spike positions and ranges until optimum simulation of the sample channel spectra is achieved by increasing the SNR to maximum value.

Although SNR is an important quantity for measuring the quality of spectra, it does not give any information about the impact these spectral handling techniques have on the retrieved spectral parameters. Because techniques 1–6 involve modifying either the

[2]Calculated as: [(tech. 6 SNR increase) – (tech. 1 SNR increase)]*100/(tech. 1 SNR increase).

Fig. 7. Change in SNR with interferogram editing techniques for samples 4 and 5.

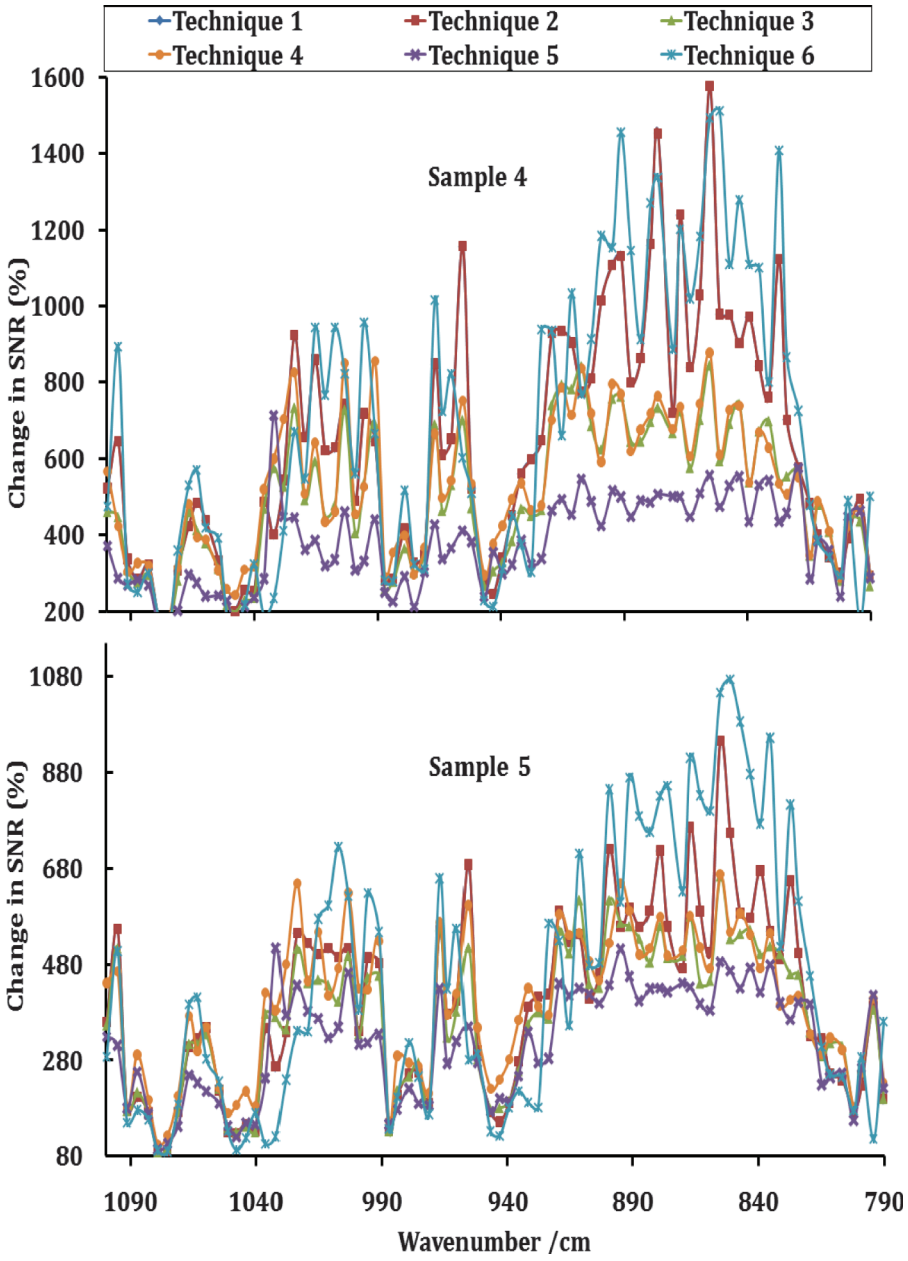

sample or the background interferogram, which alters its information content, another method to compare and test handling techniques with respect to the retrieved spectral parameters was performed.

Measured spectra are usually used in multispectrum fitting software to retrieve spectral parameters. The fit quality and accuracy of retrieved parameters can be used as an estimate of the impact of the handling techniques on the spectra. To compare all handling techniques, eight different groups of spectra were created, each containing the same seven spectra in Table 2 but processed with a different channel spectra handling technique. The first group (0) contains the seven original spectra; the second to the seventh groups (1–6) contain the same samples handled with techniques 1–6, consecutively (see Table 1). Group seven (7) contains again the original spectra but fitted using channel spectra parameters calculated from the program as detailed in Sect. 2.2. Because fitting a wide spectral range for channel spectra is difficult, the full spectral range (794.9–827.3 cm^{-1}) of interest was divided into six small spectral ranges (~5.4 cm^{-1} each) and fitted separately. The fit quality is represented by the standard deviation (STDV) of the measured spectra from the modeled fit solutions listed in Table 4 and the residuals for region 1 shown in Figs. 9 and 10. Both indicate that technique 7 has much lower STDV and therefore has better fit.

The percentage changes between the fit residual STDV for spectra handled for channel spectra from original spectra fit residual STDV in each of the six ranges considered in our discussion are presented in Table 5 and Fig. 11. Technique 7 (fitting channel spectra) shows the largest reduction in the STDV of the modeled solution, indicating that this technique reproduces the original spectra better than other techniques. Figure 11 also shows that the amount by which the fit STDV is reduced can vary considerably with the spectral range for all techniques except for technique 7. For all techniques, the STDV values plotted in Fig. 11 vary in a

Fig. 8. Change in the SNR with interferogram editing techniques for samples 6 and 7.

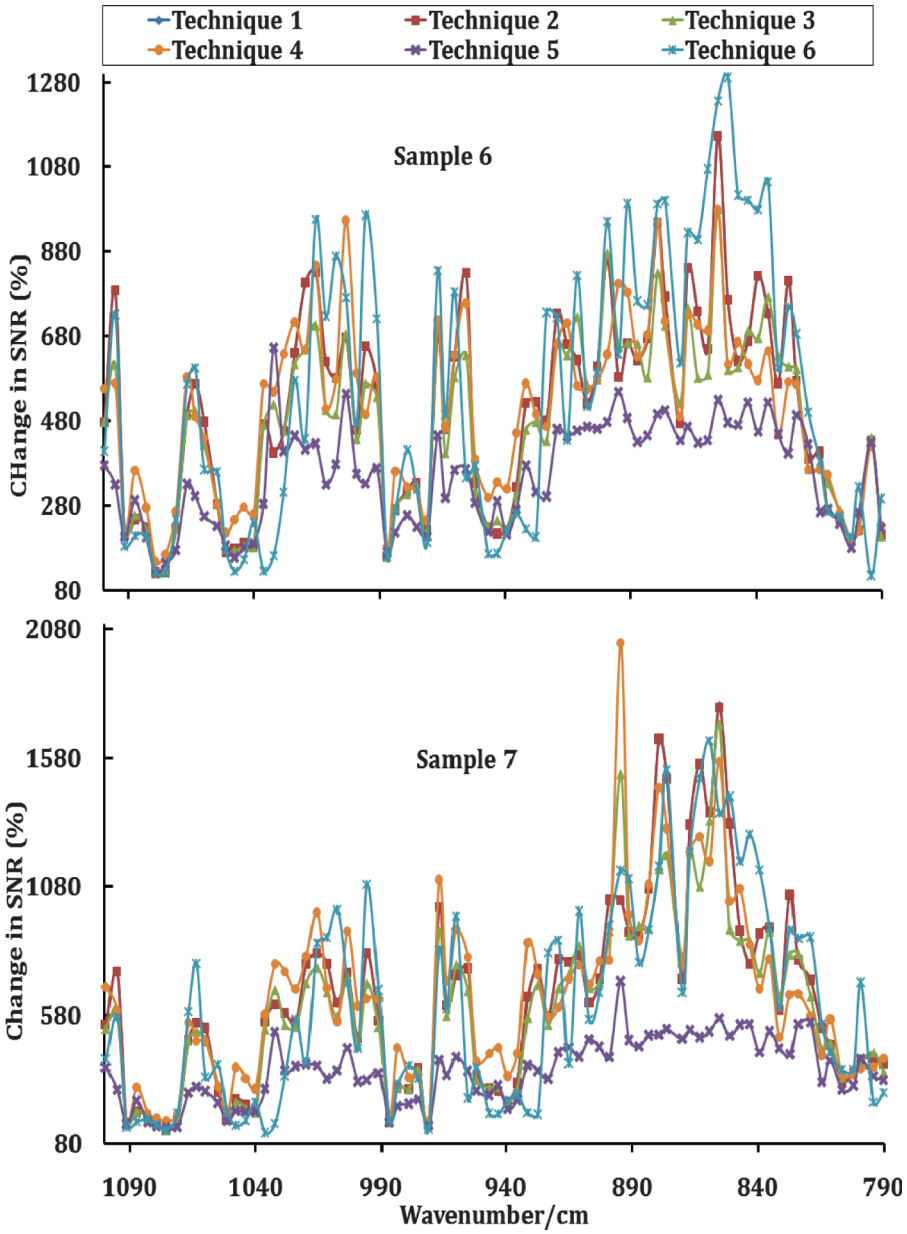

Table 4. STDVs of spectral fits in different channel handling techniques.

Range Group	Range 1 (794.9–800.5) cm^{-1}	Range 2 (800.5–806) cm^{-1}	Range 3 (805.5–811.5) cm^{-1}	Range 4 (811.4–816.5) cm^{-1}	Range 5 (816.3–821.5) cm^{-1}	Range 6 (821.4–827.5) cm^{-1}	Full range STDV
Group 0	2.189	2.166	2.122	2.109	2.062	2.074	2.138
Group 1	1.045	1.053	0.877	0.830	0.663	0.583	0.872
Group 2	1.045	1.053	0.877	0.830	0.633	0.583	0.872
Group 3	1.053	1.029	0.807	0.868	0.706	0.647	0.876
Group 4	0.997	1.037	0.811	0.838	0.722	0.677	0.873
Group 5	0.992	1.187	0.911	0.981	0.737	0.719	0.941
Group 6	1.068	1.114	0.860	0.785	0.596	0.526	0.890
Group 7	0.521	0.594	0.517	0.561	0.523	0.487	0.622

Note: All values in percent.

sinusoidal fashion similar to channel spectra, which could be an indication of residual unaccounted channel spectra. However, the accuracies of the retrieved line parameters, such as line position, intensity, and air broadening, are the main objective of the fit. The average percentage deviations from HITRAN values for lines position, intensities, and air-broadening coefficients retrieved using spectra handled by each technique are listed in Table 5.

Fig. 9. Seven original spectra and their fitting residuals when techniques 1 and 2 are used to handle channel spectra.

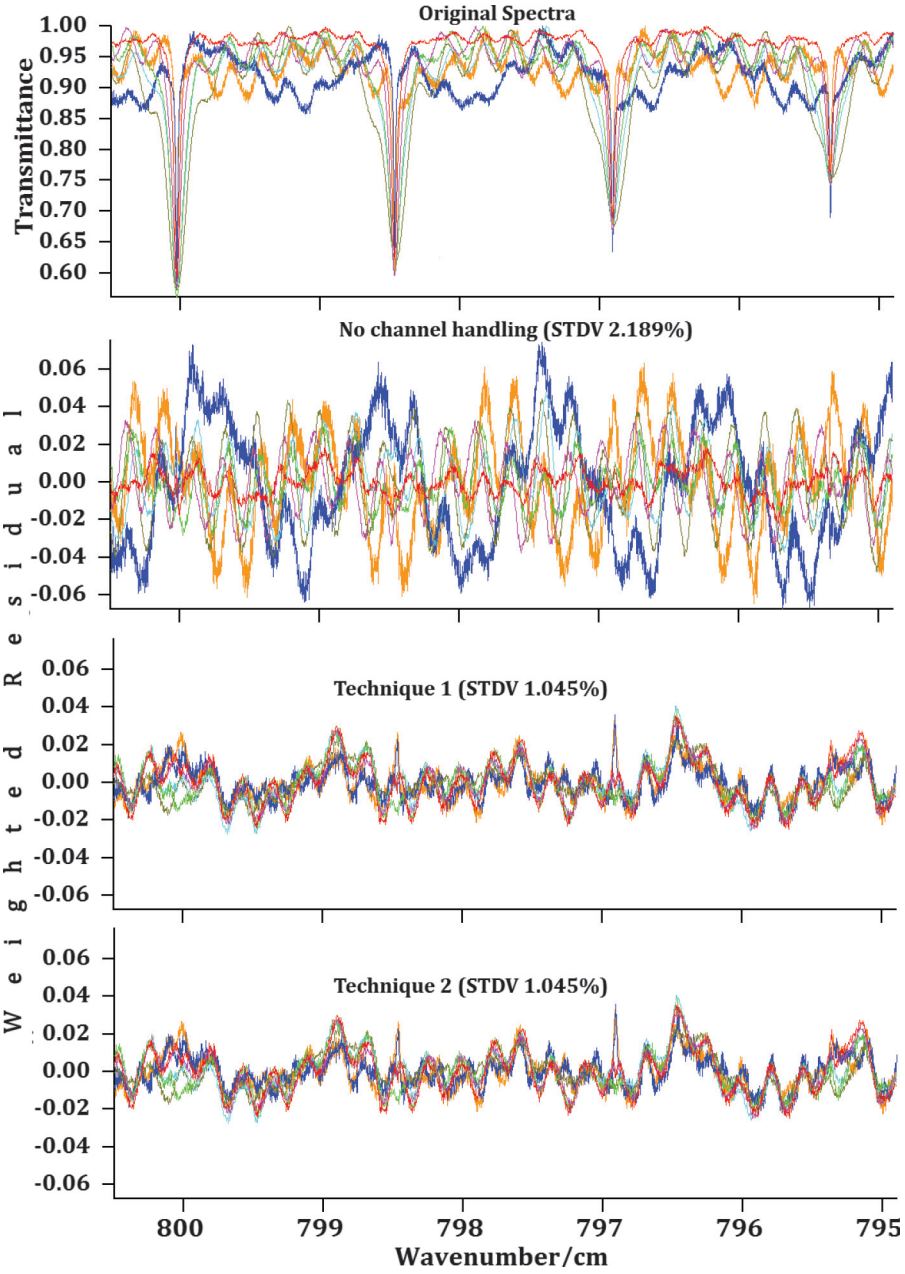

Line positions did not show noticeable changes from HITRAN [15] values and retrieved. However, for intensity and air broadening, there were observable changes from HITRAN. Regarding intensity, retrieved lines using technique 7 spectra was the most accurate and on average deviated 3.28% from HITRAN. Similarly, retrieved air broadening using technique 7 spectra were the most accurate to HITRAN with 4% average deviation. Knowing that HITRAN [15] uncertainty limits for intensities are ≥2% and <5%, and ≥5% and <10% for air-broadening, these results indicate that the channel handling technique did not cause any degradation in the quality of retrieved spectral parameters. The deviation of individual lines retrieved intensity and air-broadening from HITRAN values using different channel spectra handling techniques are shown in Fig. 12. An examination of Table 5 and Fig. 12 indicates that all techniques reduce the retrieved intensity considerably with the exception of technique 7, which also produced air-broadening coefficients that are more accurate compared to HITRAN.

5. Conclusion

Seven carbon dioxide spectra recorded at the CLS synchrotron facility were used to test seven different channel handling techniques. Six of these techniques used interferogram editing, and were tested using a LabVIEW program designed to calculate the SNR of the channel handled spectra. The results showed that using a synthetic background produced from the sample interferogram to simulate the channel spectra yielded a higher increase in SNR when compared to other interferogram editing techniques. However, testing the different handling techniques using a nonlinear least square multispectrum fitting program showed that technique 7 (channel spectra fitting) resulted in

Fig. 10. Fitting residuals for spectra handled by techniques 3–7.

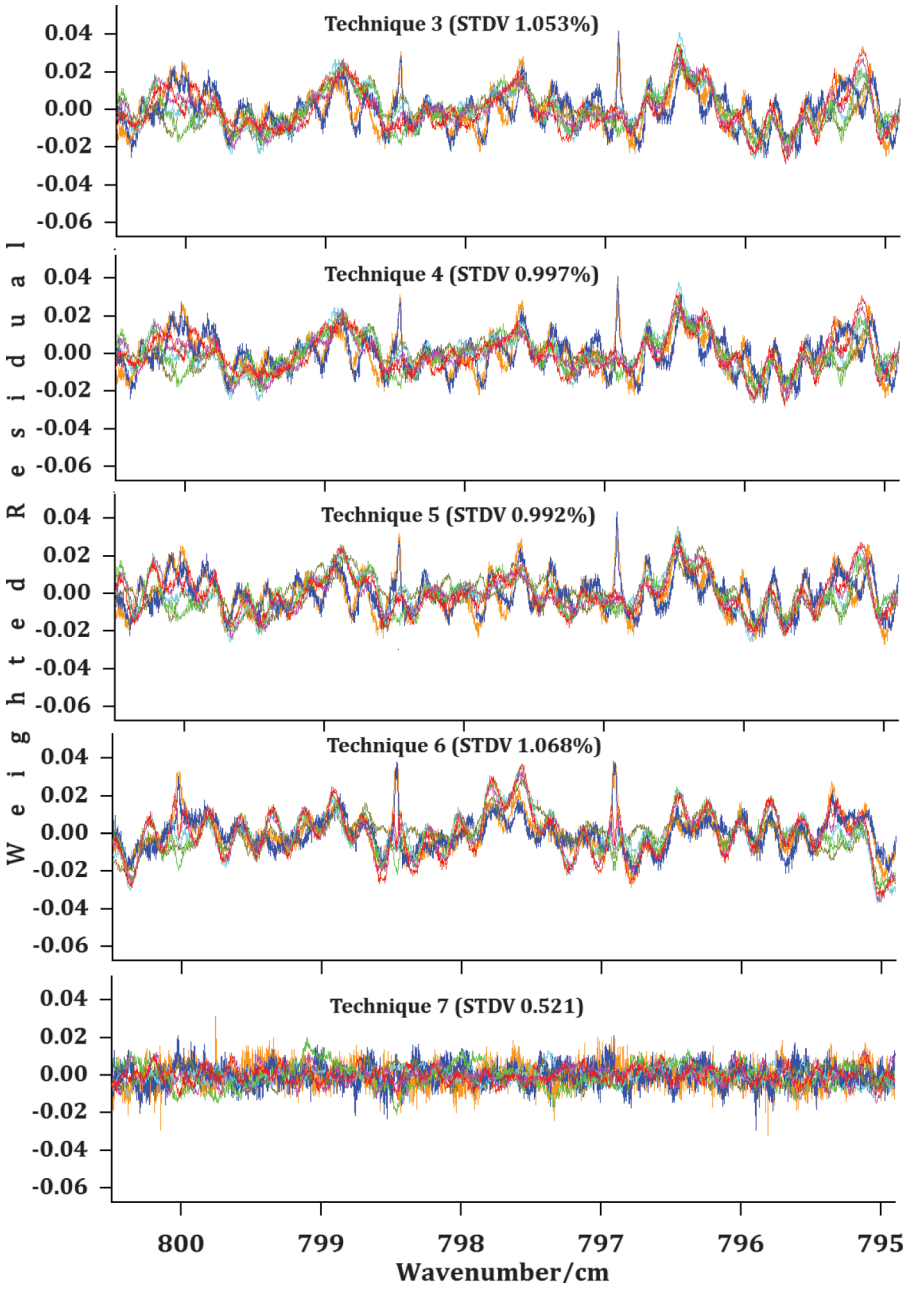

Table 5. Average deviation of retrieved line parameters from HITRAN values.

	Technique No.							
Parameter	0	1	2	3	4	5	6	7
Position × 10^{-5}	704	855	855	680	858	779	425	400
Intensity	5.23	35.4	35.4	35.1	34.3	34.5	34.1	3.29
Air broadening	8.09	12.4	12.4	12.3	14.4	15.7	12.7	4.01

Note: All values are averages of [(retrieved line – HITRAN)/HITRAN]*100 in percent.

fitting quality significantly better and consistent throughout the spectral range. The intensities retrieved from the fits when compared to HITRAN [15] values showed that all interferogram editing techniques cause significant reduction in the retrieved line intensities. Technique 7 provides intensities different by 3.29% from the HITRAN values. Because the HITRAN database [15] lists the uncertainty in line intensities for this band to be ≥2% and <5%, these results that are in agreement with the current database values. Also using spectra handled by technique 7, the measured air-broadening results were within 4.01% of the HITRAN values, which are within the listed uncertainty in HITRAN [15].

Because technique 7 (channel spectra fitting) using narrow spectral ranges produces better fits and line parameters, compared to HITRAN [15], than other techniques, it is the recommended technique. However, the narrow spectral range requirement could be laborious when wide ranges need to be analyzed for a large number of spectra. For example, the CO_2 laser band I from 920 to 993 cm^{-1} would be divided into 13 sections and, if the fit has 24 spectra, hence over 300 spectral files. The more serious effect of this limited range requirement arises from the inability to

Fig. 11. Percentage change in the fits STDV for different channel handling techniques from no channel handling case in all spectral ranges.

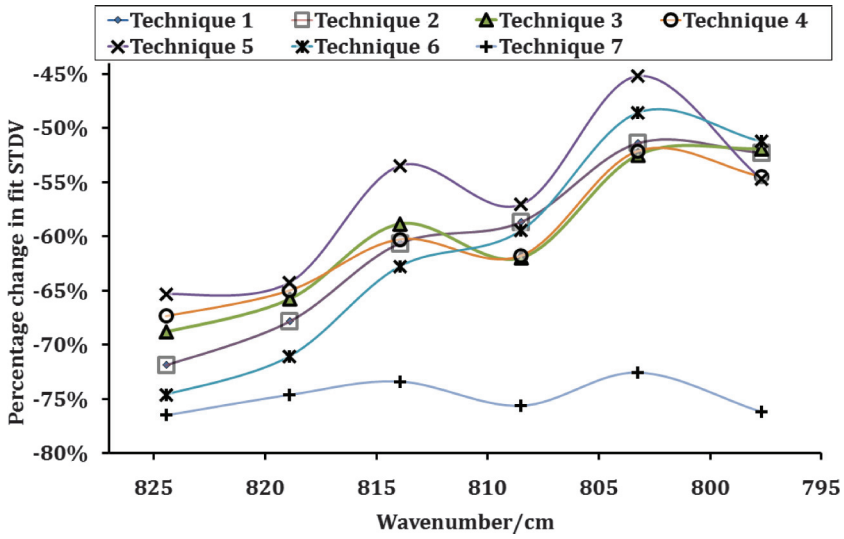

Fig. 12. Difference between results retrieved using different channel handling techniques and HITRAN [1] data listed spectral line rotational quantum number *J* for (A) line intensity and (B) air-broadening coefficient.

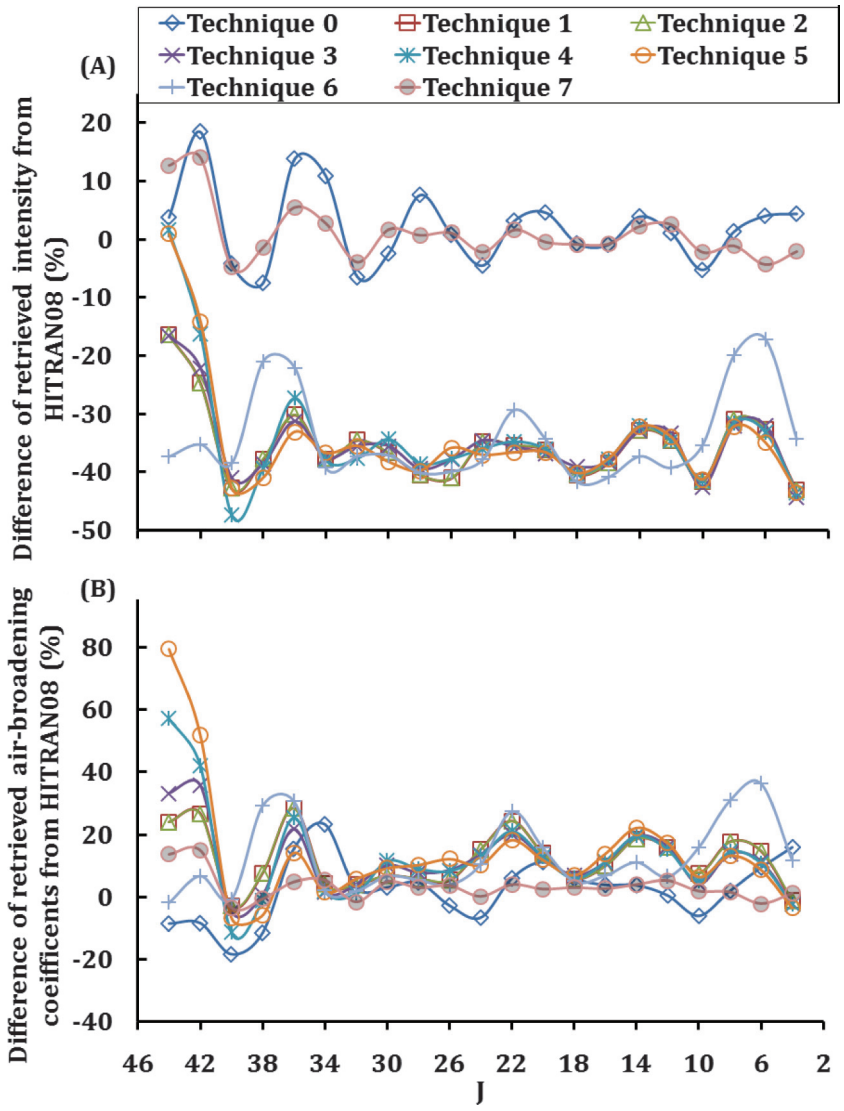

analyze the complete band and use constraints to model the band instead of individual line parameters, which is useful in retrieving parameters for weak bands [16]. Therefore, improvements for technique 7 to widen the spectral requirement while keeping its channel reduction and accurate retrieval of spectral parameters would be valuable.

Acknowledgements

The authors wish to thank Canadian Light Source, which is supported by the Natural Sciences and Engineering Research Council, National Research Council, Canadian Institutes of Health Research, and the University of Saskatchewan, where the spectra were recorded. APC acknowledges the support received from the Natural Sciences and Engineering Research Council of Canada. AI and APC are thankful to P. Teillet for his technical comments and advice throughout the duration of this project.

References

1. L. Vernoud, H.A. Bechtel, F. Borondics, and M.C. Martin. *In* WIRMS (2009) 5th International Workshop on Infrared Microscopy and Spectroscopy with Accelerator Based Sources. *Edited by* A. Predoi-Cross and B.E. Billinghurst. AIP, Alberta (Canada). 2010. pp. 36–38.
2. G.L. Carr, O. Chubar, and P. Dumas. *In* Spectrochemical analysis using infrared multichannel detectors. *Edited by* R. Bhargava and I. Levin. Blackwell Pub., Ames, Iowa. 2005. p. 60.
3. T.E. May, J.C. Bergstrom, L.O. Dallin, and D.R.T. Appadoo. 33rd International Conference on Infrared, millimetre and Terahertz waves (IRMMW-THz). Pasadena, CA. 2008. pp. 1–3.
4. T. Hirschfeld and A.W. Mantz. Appl. Spectrosc. **30**, 552 (1976). doi:10.1366/000370276774456813.
5. T. Hirschfeld. Appl. Opt. **17**, 1400 (1978). doi:10.1364/AO.17.001400. PMID:20197993.
6. G.C. Mellau and B.P. Winnewisser. *In* Laboratory and Astronomical High Resolution Spectra, Vol. 81. *Edited by* S.J. Sauval, R. Blomme, and N. Grevesse. 1995. pp. 138–139.
7. A.K. Atakan, W.E. Blass, and D.E. Jennings. Appl. Spectrosc. **34**, 369 (1980). doi:10.1366/0003702804730321.
8. M.F. Faggin and M.A. Hines. Rev. Sci. Instrum. **75**, 4547 (2004). doi:10.1063/1.1804987.
9. D.A. Naylor, A.A. Schultz, and T.A. Clark. Appl. Opt. **27**, 2603 (1988). doi:10.1364/AO.27.002603. PMID:20531799.
10. A.M.A. Pistorius and W.J. DeGrip. Vib. Spectrosc. **36**, 89 (2004). doi:10.1016/j.vibspec.2004.04.001.
11. P.R. Griffiths and C. Homes. *In* Handbook of vibrational spectroscopy. *Edited by* J.M. Chalmers and P.R. Griffiths. J. Wiley, New York. 2002. pp. 326–336.
12. D.C. Benner, C.P. Rinsland, V.M. Devi, M.A.H. Smith, and D. Atkins. J. Quant. Spectrosc. Radiat. Transfer, **53**, 705 (1995). doi:10.1016/0022-4073(95)00015-D.
13. M.A.H. Smith, D.C. Benner, A. Predoi-Cross, and V.M. Devi. J. Quant. Spectrosc. Radiat. Transfer, **110**, 639 (2009). doi:10.1016/j.jqsrt.2009.02.015.
14. J.-J. Max and C. Chapados. Appl. Spectrosc. **62**, 1167 (2008). doi:10.1366/000370208786049132. PMID:18926028.
15. L.S. Rothman, I.E. Gordon, A. Barbe, et al. J. Quant. Spectrosc. Radiat. Transfer, **110**, 533 (2009). doi:10.1016/j.jqsrt.2009.02.013.
16. V.M. Devi, D.C. Benner, L.R. Brown, C.E. Miller, and R.A. Toth. J. Mol. Spectrosc. **245**, 52 (2007). doi:10.1016/j.jms.2007.05.015.